ANALYSIS, MODELING, AND SIMULATION OF THE TIDES IN THE LOXAHATCHEE RIVER ESTUARY (SOUTHEASTERN FLORIDA)

by

PETER BACOPOULOS
B.S. University of Central Florida, 2003

A thesis submitted in partial fulfillment of the requirements
for the degree of Master of Science
in the Department of Civil and Environmental Engineering
in the College of Engineering and Computer Science
at the University of Central Florida
Orlando, Florida

Fall Term
2005

ABSTRACT

Recent cooperative efforts between the University of Central Florida, the Florida Department of Environmental Protection, and the South Florida Water Management District explore the development of a two-dimensional, depth-integrated tidal model for the Loxahatchee River estuary (Southeastern Florida). Employing a large-domain approach (i.e., the Western North Atlantic Tidal model domain), two-dimensional tidal flows within the Loxahatchee River estuary are reproduced to provide: 1) recommendations for the domain extent of an integrated, surface/groundwater, three-dimensional model; 2) nearshore, harmonically decomposed, tidal elevation boundary conditions.

Tidal simulations are performed using a two-dimensional, depth-integrated, finite element-based code for coastal and ocean circulation, ADCIRC-2DDI. Multiple variations of an unstructured, finite element mesh are applied to encompass the Loxahatchee River estuary and different spatial extents of the Atlantic Intracoastal Waterway (AIW). Phase and amplitude errors between model output and historical data are quantified at five locations within the Loxahatchee River estuary to emphasize the importance of including the AIW in the computational domain. In addition, velocity residuals are computed globally to reveal significantly different net circulation patterns within the Loxahatchee River estuary, as depending on the spatial coverage of the AIW.

ACKNOWLEDGEMENT

The study presented herein is the product of my individual efforts combined with the assistance received from a number of people, to whom I would like to express appreciation and gratitude for helping me complete this work. First, I would like to thank my advisor, Dr. Scott C. Hagen, for providing me with the opportunity to pursue graduate study at the University of Central Florida. This thesis would not have been possible without his support and guidance, in addition to the knowledge and education that I received firsthand by studying under his direction. I would also like to thank Drs. Manoj Chopra and Gour-Tsyh Yeh for agreeing to serve on my thesis committee and for offering a multitude of interesting and challenging courses; my Japanese lab mates, Yuji Funakoshi and Satoshi Kojima, for sharing their pleasant culture with all of us in the lab; present lab members, David Coggin and Mike Salisbury, for their perspectives and advice; former lab members, Daniel Dietsche, Ryan Murray, and Michael Parrish, for their contributions; Dr. Gordon Hu and other South Florida Water Management District (SFWMD) members for coordinating a boat trip (site visit) along the Loxahatchee River; Dr. Alan Zundel and his students in the Environmental Modeling Research Laboratory at Brigham Young University for providing me with specialized training in mesh generation; and the University of Central Florida campus and community for making my graduate education quite an enjoyable experience.

In the grander scheme of things, I am very fortunate to have been blessed with a loving and supporting family. I send the deepest appreciation to my parents for their many sacrifices and for instilling the principles and values that have allowed me to succeed in life. To my twin

brother, many thanks for being there during the good times and for helping me through the rough times. It is through our continued efforts to help each other that we grow stronger individually and together as a family unit.

This study is funded in part by the SFWMD under Contract No. CC11704A and the Florida Department of Environmental Protection (FDEP) under Contract No. S0133. The statements, findings, conclusions, and recommendations expressed herein are those of the author and do not necessarily reflect the views of the SFWMD, FDEP, or its affiliates.

TABLE OF CONTENTS

LIST OF TABLES

LIST OF FIGURES

ABBREVIATIONS

The following abbreviations are used in this thesis:

ACR	Atlantic Coastal Ridge
ADCIRC-2DDI	Advanced Circulation Model for Oceanic, Coastal, and Estuarine Waters (Two-Dimensional, Depth-Integrated Option)
AIW	Atlantic Intracoastal Waterway
ATC	Average Tidal Cycle
BG	British Gravitational
CH3D	Three-Dimensional Model of Curvilinear Hydrodynamics
CP	Carte Parallelogrammatique
CWMA	Corbett Wildlife Management Area
FDEP	Florida Department of Environmental Protection
GWCE	Generalized Wave Continuity Equation
JDSP	Jonathon Dickinson State Park
JID	Jupiter Inlet District
LTEA	Localized Truncation Error Analysis
MLLW	Mean Lower Low Water
MSD	Mean Solar Day
MSL	Mean Sea Level
RMS	Root Mean Square
SFWMD	South Florida Water Management District
SI	Systeme Internationale d'Unites

SIMSYS-2D	Two-Dimensional, Estuarine-Simulation System
SMS	Surface-Water Modeling System
USGS	United States Geological Survey
WNAT	Western North Atlantic Tidal

CONVERSION FACTORS AND PHYSICAL CONSTANTS

All quantities presented herein are expressed in the Systeme Internationale d'Unites (SI) system of measurement. The following conversion factors, as taken from Zwillinger (2003), may be used to convert from the SI system of measurement to the British Gravitational (BG) system of measurement:

Multiply SI units	By	To obtain BG units
centimeters (cm)	0.393701	inches (in)
cubic meters (m^3)	1.307951	cubic yards (cy)
cubic meters per second (cms)	35.314670	cubic feet per second (cfs)
kilometers (km)	0.621371	miles (mi)
meters (m)	3.280840	feet (ft)
radians (rad)	57.295780	degrees (°)
square kilometers (km^2)	247.105397	acres (ac)
square kilometers (km^2)	0.386102	square miles (mi^2)

where temperature conversions follow $\theta_C = \frac{5}{9}(\theta_F - 32)$ and θ_C and θ_F are the temperatures in degrees Celsius and Fahrenheit, respectively. The following linear (nautical) measurements may aid in converting between geophysical (spherical) and Cartesian space (Zwillinger, 2003): 1° of latitude ≈ 111.0 km; 1° of longitude at 40° latitude ≈ 85.3 km. The following physical constants are included in this thesis (Zwillinger, 2003): G (gravitational constant) ≈ $(6.673 \pm 0.003) \times 10^{-8}$ $cm^3/g\ s^2$; g (acceleration due to gravity, MSL at 45° latitude) ≈ 9.806194 m/s^2.

DATUM TRANSFORMATIONS

All tidal elevations presented herein are expressed in quantities of length as measured from mean sea level (MSL). The following vertical tidal datums, as taken from the Center for Operational Oceanographic Products and Services, Published Benchmark Sheet for the Loxahatchee River, Florida (http://140.90.121.76/benchmarks/8722481.html; website accessed on September 6, 2005), may serve useful in converting from MSL to another reference of measure. Note that all vertical tidal datums listed below are referenced from mean lower low water (MLLW).

Vertical tidal datum	Elevation above MLLW (m)
Mean higher high water	0.680
Mean high water	0.635
North American vertical datum 1988	0.635
Mean tide level	0.314
MSL	0.340
Mean low water	0.047
MLLW	0.000

NOTATION

The following symbols are used in this thesis:

$A_{jk,\,jl}$ = element of the interaction matrix resulting from the interference of a satellite with the main tidal constituent;

a = offshore amplitude of the M2 tidal constituent;

C = hour angle of the Moon;

C_C = Chezy friction coefficient;

C_f = bottom friction factor;

$C_{f_{\min}}$ = minimum bottom friction factor that is approached in deep waters when the hybrid bottom friction formulation reverts to a standard quadratic bottom friction function;

$C_{\#}$ = Courant number;

c = speed of a traveling wave in shallow water;

D = depth of the vertical water column;

d_l = declination of the Moon;

E_{h_2} = horizontal eddy viscosity;

F = mutual force of attraction between two self-attracting particles;

FF = form factor;

f = Coriolis parameter;

f_{DW} = Darcy-Weisbach friction factor;

f_n = tidal constituent nodal factor;

G = universal gravitational constant;

G_n = tidal constituent phase lag on the equilibrium tide phase at the Prime Meridian;

g = acceleration due to gravity;

g_n = tidal constituent phase lag relative to some defined time zero;

H = total height of the vertical water column;

H_{break} = break depth to determine if the hybrid bottom friction formulation will behave as a standard quadratic bottom friction function or increase with water depth similar to a Manning's type bottom friction function;

H_n = tidal constituent amplitude;

$\overline{Hist}$ = time-averaged historical tidal elevation;

$\overline{Hist_{amp}}$ = average amplitude of the historical tidal signal;

$Hist_i$ = time-dependent historical tidal elevation;

h = bathymetric depth, relative to MSL;

$\overline{h}$ = mean estuarine channel depth;

i = time index;

i_{a-f} = Doodson numbers;

L = wavelength of a traveling wave;

$L_j(\phi)$ = latitude- and tidal species-dependent functions of the Newtonian equilibrium tide potential;

M_λ = depth-integrated momentum dispersion in the longitudinal direction;

M_ϕ = depth-integrated momentum dispersion in the latitudinal direction;

Mod_i = time-dependent model tidal elevation;

m = mass of a particle;

m_e = mass of the Earth;

m_l = mass of the Moon;

N = total number of terms to include in a summation;

n = tidal constituent index;

n_M = Manning's friction factor;

$O(t)$ = time-series observed tidal elevations;

$P_n(x)$ = Legengre polynomials of order n for variable x;

p_S = atmospheric pressure at the free surface;

R = radius of the Earth;

R^2 = coefficient of determination;

RAY = Rayleigh criterion factor;

$\|RMS\|$ = normalized RMS error;

r = distance of separation between two self-attracting particles;

$r_{jk,\,jl}$ = ratio of the equilibrium amplitudes of the satellite tidal constituents to those of the major contributors;

r_l = distance of separation between the Earth and Moon;

$S(t)$ = time-series meteorological residual;

$T(t)$ = time-series resynthesized tidal elevations;

T_n = tidal constituent period;

T_{span} = time span of a tidal record to be analyzed;

t = time;

t_0 = reference time;

U = depth-integrated velocity in the longitudinal direction;

u_n = tidal constituent equilibrium argument;

V = depth-integrated velocity in the latitudinal direction;

V_c = volume of water contained in channels at MSL;

V_n = equilibrium tidal constituent phase lag relative to some defined time zero;

V_s = volume of water stored between mean high and low water in tidal flats and marshes;

x = longitudinal axis of the estuary;

x' = longitudinal component of horizontal (CP) space;

y' = latitudinal component of horizontal (CP) space;

Z_0 = tidal resynthesis term representative of local MSL;

α = effective Earth elasticity factor;

$\alpha_{jk,\,jl}$ = phase corrections for the satellite tidal constituents;

γ = dimensionless parameter that describes how quickly the bottom friction factor increases as water depth decreases;

Δ_1 = astronomical constant involving the masses and distances associated with a celestial system;

Δ_{jkl} = phase difference between the satellite tidal constituents and the major contributors;

Δt = time step;

Δx = nodal spacing;

ζ = free surface elevation, relative to MSL;

η = Newtonian equilibrium tide potential;

θ = dimensionless parameter that establishes how rapidly the bottom friction factor approaches its upper and lower limits;

θ_C = temperature in degrees Celsius;

θ_F = temperature in degrees Fahrenheit;

λ = degrees longitude (east of Greenwich positive);

λ_0 = longitudinal center of the CP projection;

ρ_0 = reference density of water;

σ_n = tidal constituent frequency;

τ_0 = GWCE weighting parameter;

$\tau_{S\lambda}$ = applied free surface stress in the longitudinal direction;

$\tau_{S\phi}$ = applied free surface stress in the latitudinal direction;

τ_* = quadratic bottom stress;

ϕ = degrees latitude (north of equator positive);

ϕ_0 = latitudinal center of the CP projection;

$\left|\overline{\varphi}\right|$ = absolute average phase error;

φ_n = tidal constituent phase lag relative to some defined time zero;

Ω = angular speed of the Earth;

Ω_P = gravitational potential at a point P on the Earth's surface;

ω_n = tidal constituent angular speed.

CHAPTER 1. INTRODUCTION

The Loxahatchee River estuary, located on the east coast of Florida within northern Palm Beach and southern Martin counties, empties into the Atlantic Ocean through Jupiter Inlet (Figure 1.1). The estuarine system is comprised of three major tributaries: the Northwest Fork (Loxahatchee River); the North Fork; the Southwest Fork. The Atlantic Intracoastal Waterway (AIW) runs parallel to the coastline and intersects the Loxahatchee River between the central embayment and Jupiter Inlet.

Human activities have altered the natural drainage patterns occurring within the Loxahatchee River estuary. Prior to development, nearly level, poorly drained lands, which were subject to frequent flooding, characterized most of the watershed region. As a result, a primary and several secondary drainage systems and associated water-control facilities were constructed in order to transform the Loxahatchee River watershed into an area suitable for agricultural and residential development. Some notable structural changes that are considered here include excavation and stabilization of Jupiter Inlet, dredging, filling, and bulkheading within the estuary and along the Loxahatchee River, and the construction of major canals and water-control structures. Over a century of water-control and structural modifications made to this estuarine system has led to changes in the quality, quantity, timing, and distribution of surface water inflows delivered to the Loxahatchee River estuary, in addition to lowering the groundwater table within the surrounding watershed (McPherson and Sabanskas, 1980).

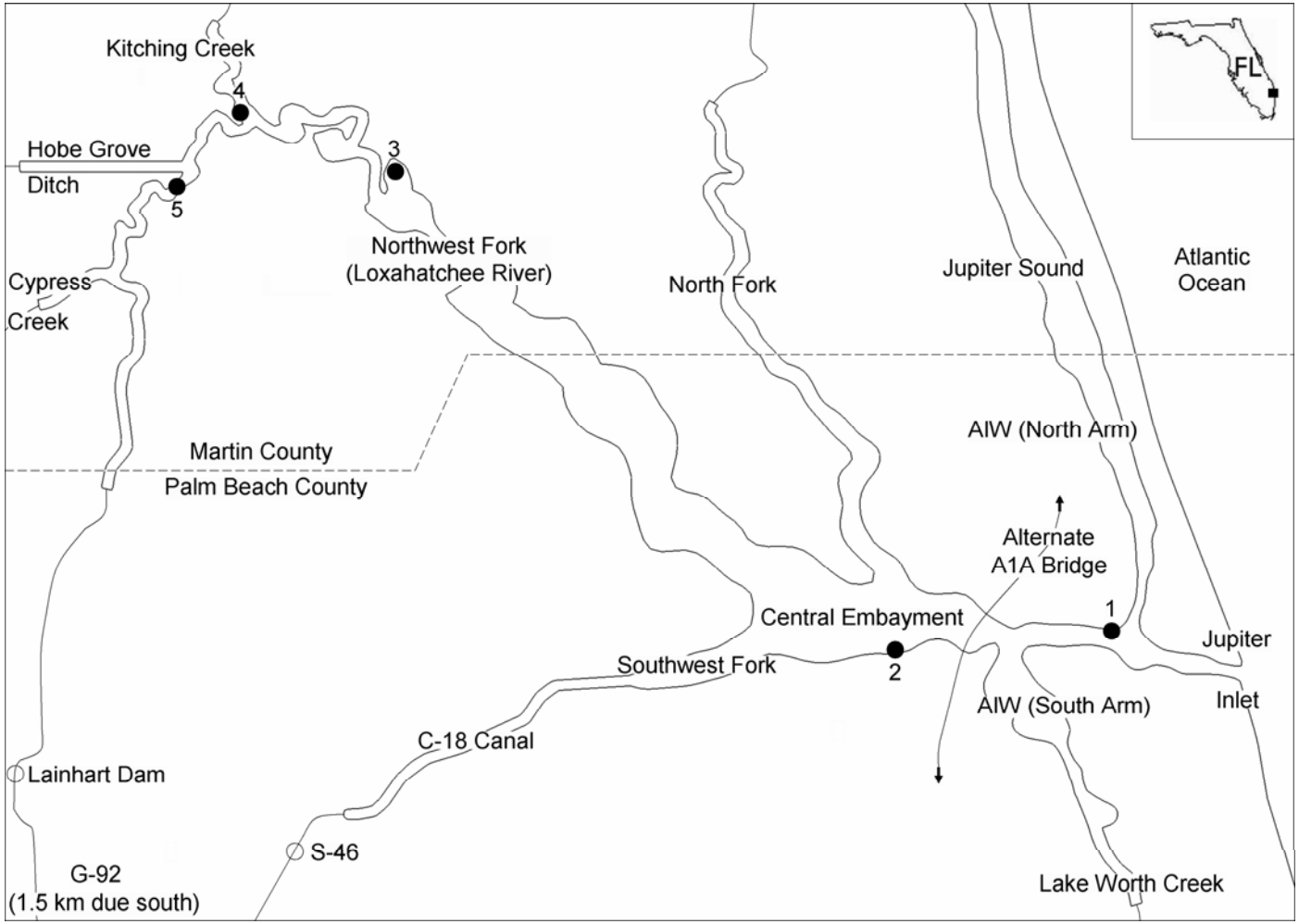

Figure 1.1. Map of the Loxahatchee River estuary, including the locations of the five water level gaging stations (Coast Guard Dock, Pompano Drive, Boy Scout Dock, Kitching Creek, and River Mile 9.1, corresponding to the circles numbered 1-5, respectively) situated within its interior.

Coastal development has also greatly affected the hydrology of the Loxahatchee River estuary. Historical evidence indicates that the mouth of the estuary, Jupiter Inlet, has been opened and closed many times in the past as the result of natural causes. Originally, the inlet was maintained open by surface water inflows supplied not only by the Loxahatchee River, but also from Lake Worth Creek and Jupiter Sound, as located in the north and south arms of the AIW, respectively. (Refer to Figure 1.1 for a map of the Loxahatchee River estuary which highlights these two regions of the AIW.) Near the turn of the century, some of these surface water inflows were diverted by the creation of the AIW and Lake Worth Inlet and by the modification of St. Lucie Inlet (Vines, 1970). Subsequently, Jupiter Inlet remained closed much of the time until 1947, except when periodically dredged. Since 1947, the inlet has been kept open to the sea through regular dredging (McPherson et al., 1982).

As a consequence of these drainage-basin alterations, inlet modifications, and dredging activities, groundwater levels within the adjacent floodplains have been lowered and freshwater river inflows feeding the estuary have been reduced or altered in direction or period of flow (McPherson and Sabanskas, 1980). This has led to the upstream migration of saltwater into the historical freshwater reaches of the Loxahatchee River, which is the likely cause of altered floodplain cypress forest communities found along the Northwest Fork and some of its tributaries. Mangroves are replacing cypress forest and areas of mixed swamp hardwoods have reacted to different degrees to the saltwater stresses. Russell and McPherson (1984) conducted an intensive study to investigate the relationship between salinity distribution and freshwater river inflow in the Loxahatchee River estuary, using tidal, salinity, and river-discharge data corresponding to the dates between 1980 and 1982. More recently, studies conducted by Dent and Ridler (1997) indicate that freshwater river inflows delivered to the Northwest Fork are

insufficient to maintain freshwater conditions in the Loxahatchee River around the watershed areas affected by saltwater intrusion.

To this end, the South Florida Water Management District (SFWMD), in cooperation with the Florida Department of Environmental Protection (FDEP), as part of a research effort to establish minimum flows and levels for the Loxahatchee River, developed a two-dimensional, hydrodynamic/salinity model for the estuary (SFWMD, 2002). The purpose of this modeling effort was to provide predictions of the salinity expected at various locations within the estuary with respect to freshwater river inflows and tidal fluctuations (Hu, 2002). Since this estuary model did not include a groundwater component, it could not answer questions related to saltwater intrusion and the associated effects on the vegetation within the surrounding watershed. Hence, an integrated, surface/groundwater, three-dimensional model has been developed to simulate river and estuarine hydrodynamics and salt transport in both surface water and groundwater for the Loxahatchee River estuary. It is the purpose of the SFWMD to implement this integrated, three-dimensional estuary model in order to provide salinity predictions within the Loxahatchee River and vegetation root zone of the adjacent floodplains. As a result, saltwater intrusion on the Northwest Fork and the feasibility of a saltwater barrier on the Loxahatchee River will be more thoroughly investigated.

The primary focus of the present study concentrates on generating nearshore, tidal elevation data which will be used to force the open-ocean boundary of the integrated, three-dimensional estuary model. A large-scale computational domain that describes the western North Atlantic Ocean, Gulf of Mexico, and Caribbean Sea is extended to include the Loxahatchee River estuary and a limited portion of the AIW. This initial version of the finite element mesh is applied in preliminary tidal simulations, using a two-dimensional, depth-

integrated, finite element-based code for coastal and ocean circulation, ADCIRC-2DDI, for computations. A statistical analysis of the errors between model output and historical data at five locations within the Loxahatchee River estuary (see Figure 1.1) provides absolute average phase errors and goodness-of-fit measures that indicate a need for improvement.

Model calibration then follows with adjustments in bottom friction parameterization and the application of (advective) freshwater river inflows; however, this sensitivity analysis fails to improve the model response within the Loxahatchee River estuary to within acceptable levels. Therefore, a second generation of the finite element mesh is produced in order to extend the AIW to the north and south from the current domain extent, and to include the description of Fort Pierce and St. Lucie Inlets and Lake Worth Inlet to the north and south, respectively, of Jupiter Inlet. Tidal simulations follow and computed phase and amplitude errors highlight the importance of including the AIW in the computational domain.

Finally, globally computed velocity residuals reveal a significant net circulation within the north arm of the AIW in relation to the weak patterns in net mass transport observed through the south arm of the AIW. A final version of the finite element mesh is then produced by truncating the north and south arms of the AIW at a reasonable distance from Jupiter Inlet, whereby reasonable refers to providing enough spatial coverage of the AIW to accurately reproduce the circulation patterns within the Loxahatchee River estuary without excessively increasing the computational requirement of the integrated, three-dimensional estuary model.

CHAPTER 2. TIDAL ANALYSIS

It is assumed that in the following discussion, a general knowledge of the tides is understood; however, to facilitate this review on tidal analysis, the works of Darwin (1911), Doodson (1921), Schureman (1941), Cartwright and Taylor (1971), Cartwright and Edden (1973), Knauss (1978), Schwiderski (1980), Pugh (1987), Reid (1990), Deacon (1997), Cartwright (1999), Open University (2000), and Pugh (2004) may be referenced to provide a thorough account of the equilibrium tides. It is noted, however, that while equilibrium tidal theory provides insight into the instantaneous response of the sea surface due to the tide-generating forces, disagreement exists between the equilibrium tides and observed tidal heights. These discrepancies are due to the incomplete description of the tides as offered by equilibrium tidal theory alone. Thus, a dynamic theory of the tides which recognizes the relationship between the periodic external forces and the natural frequencies and frictional characteristics of the interconnected ocean basins was established. More detailed explanations regarding dynamical oceanography and real ocean tides can be found in Darwin (1911), Proudman (1953), Defant (1960), Dietrich and Kalle (1963), McLellan (1965), Macmillan (1966), Neumann and Pierson (1966), Phillips (1966), Pickard (1975), LeBlond and Mysak (1978), Schwiderski (1980), and Reid (1990).

As a brief review of the various tides that are observed on Earth, the dominant periodic geophysical forcing is the variation of the gravitational field as exerted on the Earth's surface and as caused by the recurring motions of the Earth-Moon and Earth-Sun systems. (Refer to Appendix A for an outline of the formal mathematical development of gravitational forces and the equilibrium tide as based on potential theory.) Movements due to these astronomically

induced gravitational forces are called either gravitational or, more usually, astronomical tides. Further, these gravitational body forces act directly on deep oceanic waters. Tidal effects in coastal regions, however, are not directly forced by these astronomically induced gravitational forces, and as a result, tides near the coast arise as a side effect of deep oceanic variability, propagating through shallower coastal waters as a wave or a combination of waves. There are also much smaller movements due to regular meteorological forces; these are called either meteorological or, more usually, radiational tides.

Tidal analysis, in the most basic sense, is a special case of time-series study; the idea is to condense a long-term record of observations into a brief collection of time-invariant constants. Due to the regularity of the tide-generating forces (e.g., those resulting from the relative [to Earth] motions of the Moon and Sun), periodicities contained within a tidal record may be extracted in order to describe the tidal displacement at a location as a sum of the associated harmonics. For a historical review, various methods of such harmonic analyses, as devised by Darwin (1911), Doodson (1928), and Horn (1960), are primarily aimed at determining the amplitude and phase properties of the predominant harmonics. More recently, attempts have been made to evaluate the contribution of non-tidal phenomena present in the record of observations in order to provide a quantitative estimate of the variability in the tidal record (Munk and Cartwright, 1966). The following section on tidal analysis covers a brief review of the mathematics involved with the analysis of the tides, a discussion regarding harmonic constants and their role in representing the tides, and an example harmonic analysis procedure, as applied to the historical water level data that are used in the present study.

Specialized techniques have been devised to take advantage of the deterministic nature of the tides. In classical harmonic analysis, the tidal forcing is modeled as a set of spectral lines,

and hence, Fourier series forms the basis of the harmonic analysis of the tides; a superposition of multiple sinusoidal waves, each with its own properties (e.g., interval of recurrence and those associated with the amplitude and phase of the tidal component), to form a total tidal signal. Therefore, tidal variations can be represented by a finite number N of harmonic terms of the form (Cartwright and Taylor, 1971):

$$H_n \cos(\omega_n t - g_n) \quad \text{(2.1)}$$

where n = component index; H_n = component amplitude; ω_n = component angular speed = $2\pi/T_n$; T_n = component period; g_n = component phase lag relative to some defined time zero (commonly taken as the phase lag on the equilibrium tide phase at the Prime Meridian, in which case it is called G_n); t = time.

Due to the nearly linear nature of the dynamics between the tide-generating forces and the associated ocean response, it is implied then that the forced response of the ocean surface contains only those frequencies present in the tide-generating forces. Hence, use of the equilibrium tide is helpful in determining the angular speeds of the various tidal components. These are found by an expansion of the equilibrium tide into harmonic terms; the speeds of these terms are found to have the general form (Doodson, 1921):

$$\omega_n = i_a\omega_1 + i_b\omega_2 + i_c\omega_3 + (\omega_4, \omega_5, \omega_6 \text{ terms}) \quad \text{(2.2)}$$

where the values of ω_1 to ω_6 are the angular speeds related to the astronomical parameters listed in Table 2.1 and the coefficients i_a to i_c are small integers, usually in the range between -2 and 2.

Thus, a specific set of these six integers (referred to as the Doodson numbers) may be applied (through Eq. [2.2]) to the fundamental frequencies listed in Table 2.1 in order to specify a particular tidal frequency (Godin, 1972).

Table 2.1. The basic speeds and origins of the astronomical arguments that give the frequencies of the harmonic components (after Harris [1991]).

Origin	Period	Degrees per mean solar hour	Symbol
Mean solar day (MSD)	1.0000 MSD	15.0000	ω_0
Mean lunar day	1.0351 MSD	14.4921	ω_1
Sidereal month	27.3217 MSD	0.5490	ω_2
Tropical year	365.2422 MSD	0.0411	ω_3
Moon's perigee	8.85 years	0.0046	ω_4
Regression of Moon's nodes[a]	18.61 years	0.0022	ω_5
Perihelion	20942 years	–	ω_6

[a] Refer to Appendix B for an overview of nodal cycles.

At this point in the harmonic analysis, the individual harmonic components (herein referred to as tidal constituents) are derived by considering the associated periodicities of the corresponding tide-generating forces. For example, the M2 tidal constituent is representative of the semi-diurnal (with a period of 12 hours and 25 minutes) tide resulting from the Moon's revolution about the Earth in a circular orbit. The naming convention follows that the letter M represents the Moon and the number 2 indicates that the tide occurs twice a day. Similarly, the semi-diurnal tide generated by the Sun (as being on the equatorial plane of the Earth) has a

period of exactly 12 hours, and hence, the S2 tidal constituent is represented. It is noted here that the combination of these two tides (M2, S2) produces the spring-neap tidal cycle (Figure 2.1).

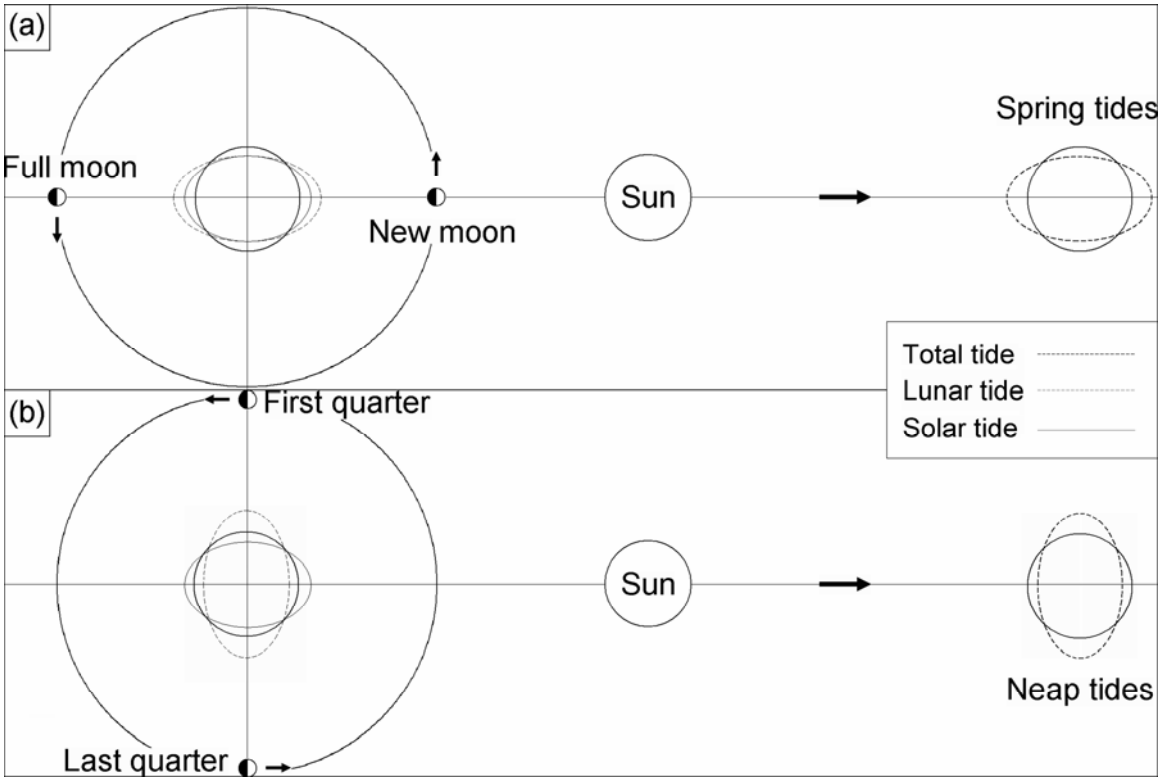

Figure 2.1. (a) Spring tide conditions when the Moon is in syzygy and (b) neap tide conditions when the Moon is in quadrature (after Pugh [2004]).

These concepts are now related to the actual movements of the Moon and Sun by considering each individual modulation (e.g., those associated with the Moon's phase, distance from Earth, and declination) as an effect produced by a separate phantom satellite (Pugh, 2004). For instance, the astronomical expressions can be expanded for the Moon's phase, distance from Earth, and declination mathematically to determine the periods and theoretical amplitudes of the extra terms. The concept is then extended to include the longer-period variations of the Moon and Sun, which results in annual, semi-annual, and diurnal tidal constituents. When this full

expansion of the equilibrium tide is done for all modulations associated with the Moon and Sun, the resulting list of tidal constituents may be very long. Nevertheless, examination of the relative amplitudes of the tidal constituents arising from the mathematical expansion of the equilibrium tide shows that only a few harmonics are dominant (Table 2.2).

Table 2.2. The dominant harmonics of the tides and their physical causes (after Reid [1990]).

	i_b	i_c	Period (MSD)	Degrees per solar hour	Equilibrium amplitude (M2 = 1.0000)	Origin
Long-period $i_a = 0$						
SA	0	1	364.96	0.0411	0.0127	Solar annual
SSA	0	2	182.70	0.0821	0.0802	Solar semi-annual
Diurnal $i_a = 1$						
Q1	-2	0	1.120	13.3987	0.0795	Lunar ellipse
O1	-1	0	1.076	13.9430	0.4151	Principal lunar
P1	1	-2	1.003	14.9589	0.1932	Principal solar
K1	1	0	0.997	15.0411	0.5838	Principal lunar and solar
Semi-diurnal $i_a = 2$						
N2	-1	0	0.527	28.4397	0.1915	Lunar ellipse
M2	0	0	0.518	28.9841	1.0000	Principal lunar
L2	1	0	0.508	29.5285	0.0238	Lunar ellipse
S2	2	-2	0.500	30.0000	0.4652	Principal solar
K2	2	0	0.499	30.0821	0.1266	Declinational lunar and solar

The line spectra of the diurnal and semi-diurnal tidal constituents are plotted in Figure 2.2, which shows the frequencies of the terms in the fuller expansion of the equilibrium tide and confirms the significance of the dominant harmonics. The frequency-dependent pattern of tidal constituents shown in Figure 2.2 can be explained in terms of Eq. (2.2). The main divisions in the pattern of tidal constituents are the number of cycles per day (governed by i_a), where each

division is called a tidal species. In the complete astronomical expansion, i_b is used to fit the monthly modulations, which varies between -5 and 5 and defines the group within each tidal species. Within each group, i_c fits the annual modulations; it also varies between -5 and 5 and is said to define the tidal constituent.

Modulations in ω_4, ω_5, and ω_6 (see Eq. [2.2]) are affected by longer-period astronomical cycles and cannot be resolved as independent harmonics from a year of observations (see Appendix B). Therefore, variations in these astronomical arguments are represented in the harmonic expansions by small adjustment factors to the amplitude and phase. These nodal adjustment factors, f_n (nodal factor) and u_n (equilibrium argument), are applied individually to the lunar tidal constituents through Eqs. (2.1) and (2.2) in order to account for the long-term nodal modulations (Cartwright and Taylor, 1971):

$$H_n f_n \cos\left[\omega_n t - \left(g_n + u_n\right)\right] \qquad (2.3)$$

It is noted that the nodal factor and equilibrium argument are set to 1.0 and 0.0, respectively, for the solar tidal constituents, as there are no nodal effects on the solar-induced tides.

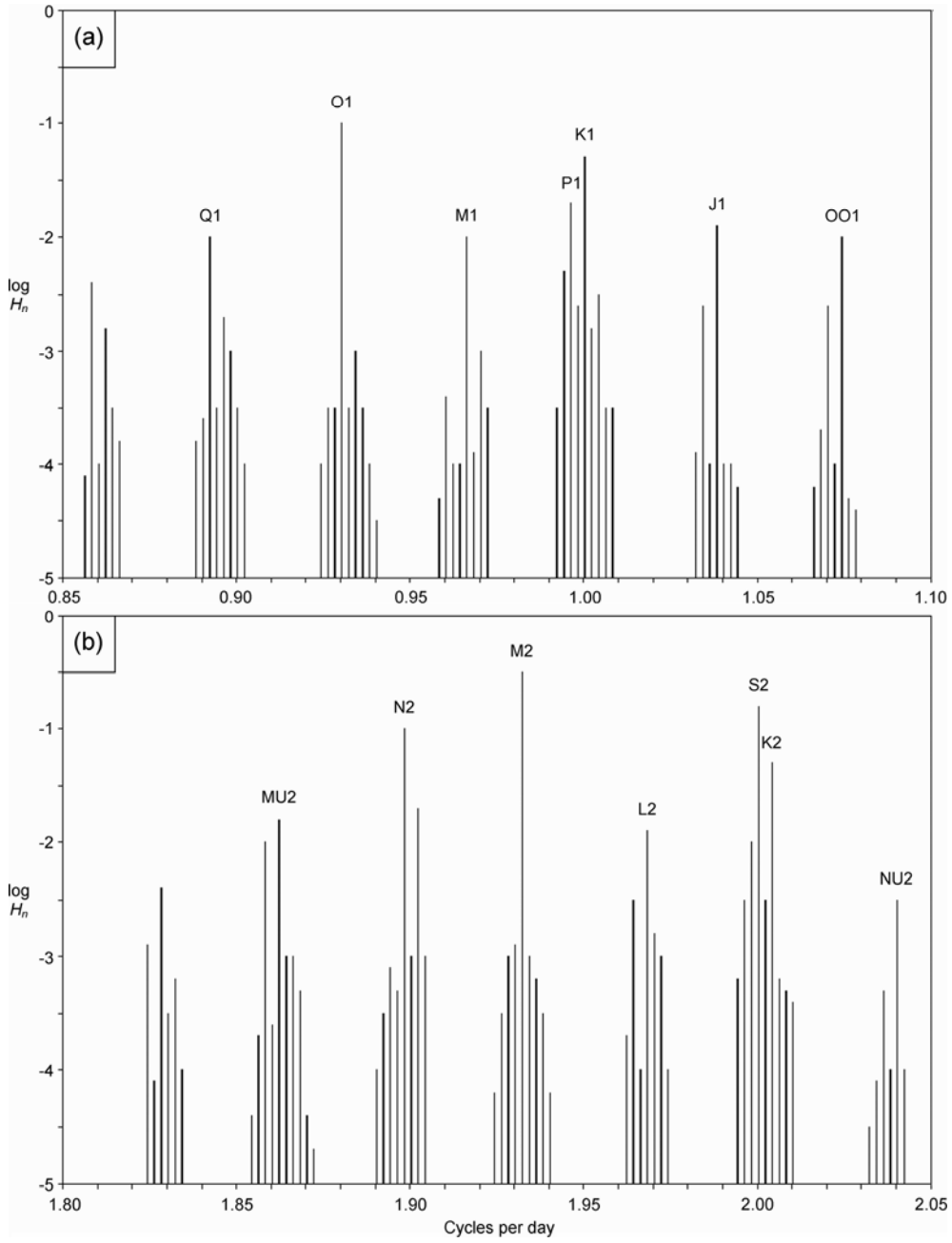

Figure 2.2. Frequency-dependent pattern of the (a) diurnal and (b) semi-diurnal tidal constituents with their associated equilibrium amplitudes plotted on a logarithmic scale (after Cartwright and Edden [1973]). Each individual vertical line represents a tidal constituent; note the clustering of tidal constituents into groups within each tidal species.

In applying the harmonic method of analysis to a tidal record, a tidal function $T(t)$ is fit to sea level observations (Godin, 1991b):

$$T(t) = Z_0 + \sum_N H_n f_n \cos[\omega_n t - g_n + (V_n + u_n)] \quad \text{(2.4)}$$

where the unknown parameters are Z_0 and the series of tidal constituent amplitudes and phases (H_n, g_n). Z_0 is included here as a variable to be fitted in the analysis, but it commonly represents local mean sea level (MSL) and is therefore a known parameter. The nodal adjustment factors are given as f_n and u_n and the terms $\omega_n t$ and V_n together determine the phase angle of the equilibrium tidal constituent. V_n is the equilibrium phase angle for the tidal constituent at the arbitrary time origin. The accepted convention is to take V_n as for the Prime Meridian and t in the standard time zone of the observation station.

A least-squares fitting procedure is then employed to determine the amplitudes and phases of the tidal constituents corresponding to the particular measurement site. This least-squares fitting procedure serves to minimize $\sum S^2(t)$, the square of the residual differences between the observed $O(t)$ and computed tidal elevations when summed over all observations (Godin, 1991b):

$$S(t) = O(t) - T(t) \quad \text{(2.5)}$$

The computational aspects of the least-squares fitting procedure involve matrix algebra and go beyond the scope of this review on tidal analysis; however, Foreman (1977) gives a thorough account of the problem formulation and matrix solution as related to fitting a tidal

function to sea level observations. It is noted, however, that the system of equations to be solved may be written schematically as follows: (observations [known]) = (equilibrium tide [known]) × (empirical constants [unknown]). Moreover, Pugh (2004) remarks on the following useful properties that the least-squares fitting procedure offers: gaps in the data are permissible; any length of data may be treated (usually complete months or years are analyzed); no assumptions are made about data outside of the interval to which the fit is made; transient phenomena are eliminated (i.e., only variations with a coherent phase at tidal frequencies are extracted); any computational time step may be employed in the analysis albeit fitting if often applied to hourly values.

There are certain rules for deciding which harmonic amplitudes and phases are to be determined from a tidal analysis. In general, the longer the length of the data record involved in the tidal analysis, the greater the number of tidal constituents may be extracted. Selection of the tidal constituents to include in the tidal analysis is often governed by the Rayleigh criterion, which requires that only harmonics separated by at least a complete period from their neighboring harmonics over the length of data available be included in the tidal analysis. For example, consider the frequencies of two individual tidal constituents, σ_0 and σ_1, and the time span T_{span} of the data record, to be analyzed. For both tidal constituents to be included in the tidal analysis, the Rayleigh criterion must be satisfied (Foreman, 1977):

$$|\sigma_0 - \sigma_1| T_{span} \geq RAY \qquad (2.6)$$

where RAY is commonly specified to be equal to unity.

Presented in an alternative way, to determine the M2 and S2 tidal constituents (with angular speeds of 28.9841 and 30.0000 degrees per hour, respectively; see Table 2.2) independently in a tidal analysis requires a data record of the following minimum length be used:

$$\frac{360^\circ}{\left(30.0000 - 28.9841\ ^\circ/\mathrm{hr}\right)} = 14.77\ \mathrm{days} \ldots\ldots\ldots\ldots\ldots\ldots\ldots\ldots\ldots\ldots\ldots\ldots\ldots (2.7)$$

where this minimum length of the data record required to resolve a pair of tidal constituents is known as the synodic period (Pugh, 2004). It is noted that in the previous case, the synodic period required to separate the M2 and S2 tidal constituents is equal to the recurrence interval of the spring-neap tidal cycle (see Figure 2.1).

For general use, an automated selection algorithm devised by Foreman (1977) is currently in place, which works as follows. First, all possible tidal constituents are gathered and listed in order of decreasing equilibrium amplitude (see Table 2.2). Less important tidal constituents (e.g., those with lesser equilibrium amplitudes) whose frequencies are less than a Rayleigh resolution limit (see Eq. [2.6]) apart from more important tidal constituents (e.g., those with greater equilibrium amplitudes) are then discarded. Finally, additional tidal constituents may be explicitly added to the list, if required.

Before continuing on with the tidal analysis, it is also necessary to satisfy another basic rule of time-series analysis, as related to the frequency at which observations are made. The Nyquist criterion states that only terms having a period longer than twice the sampling interval can be resolved. In the usual case of hourly data sampling, this shortest period is two hours, so that resolution of the twelfth-diurnal (with a period of 2 hours and 4 minutes) M12 tidal constituent would just be possible. In practice, however, this is not a severe restriction except in

very shallow waters, where sampling more frequently than once an hour is necessary to represent these shallow-water tides.

It may be discovered that due to the limiting length of the data record, many of the possible harmonics to include in the tidal analysis are not resolvable, as restricted by the Rayleigh criterion. The standard approach that is then taken to deal with this issue is to form clusters containing all of the tidal constituents with the same first three Doodson numbers (see Eq. [2.2]). The major contributor (e.g., the tidal constituent with the greatest equilibrium amplitude) lends its name to the cluster and the remaining contributors are called satellite tidal constituents. The tidal analysis, using these main and satellite tidal constituents, then continues (as described by Foreman [1977]) in the following manner. The Rayleigh criterion is applied to the frequencies of the main tidal constituents to determine their inclusion in or omission from the tidal analysis. A least-squares fit is made between the tidal function (using only the main tidal constituents) and sea level observations to obtain the apparent amplitudes and phases; however, since these results are due to the cumulative effect of all of the tidal constituents included in the clusters, an adjustment must be made to determine the contributions due to the main tidal constituents alone. In order to make these nodal modulation corrections (see Eq. [2.3]) to the main tidal constituents, it is necessary to know the relative amplitudes and phases of the satellite tidal constituents contained within the respective clusters. As is commonly done, it is assumed that the same relationship that is found with the equilibrium tide holds for the actual tide (i.e., the equilibrium amplitude ratio of a satellite to its main tidal constituent is assumed to be equal to the actual amplitude ratio, and the difference in equilibrium phase between a satellite and its main tidal constituent is assumed to be equal to the actual phase difference).

Due to the presence of satellite tidal constituents in a given cluster, it is known from equilibrium tidal theory that the analyzed signal found at the frequency of the main tidal constituent σ_j actually results from:

$$H_j \sin\left(V_j - g_j\right) + \sum_k A_{jk} H_{jk} \sin\left(V_{jk} - g_{jk}\right) + \sum_l A_{jl} H_{jl} \cos\left(V_{jl} - g_{jl}\right) \quad \ldots\ldots\ldots\ldots\ldots\ldots (2.8)$$

for the diurnal and terdiurnal (occurring three times a day) tidal constituents, and:

$$H_j \cos\left(V_j - g_j\right) + \sum_k A_{jk} H_{jk} \cos\left(V_{jk} - g_{jk}\right) + \sum_l A_{jl} H_{jl} \sin\left(V_{jl} - g_{jl}\right) \quad \ldots\ldots\ldots\ldots\ldots\ldots (2.9)$$

for the annual, semi-annual, and semi-diurnal tidal constituents (Cartwright and Taylor, 1971). The single *j* subscripts refer to the main tidal constituents while the multiple *jk* and *jl* subscripts refer to the satellite tidal constituents originating from the second- and third-order terms of the tidal potential, respectively (see Appendix A). $A_{jk,jl}$ is the element of the interaction matrix resulting from the interference of a satellite with the main tidal constituent (Foreman, 1977).

It is the convention in tidal analysis, and an assumption made in the least-squares fitting procedure, that all tidal constituents arise through a cosine term with positive amplitude; however, the diurnal and terdiurnal tidal constituents, assuming that they are due to second-order terms in the tidal potential, actually arise through a sine term with a (possible) negative amplitude. Hence, a phase correction of either $-\frac{1}{4}$ or $-\frac{3}{4}$ cycles is necessary:

$$H_j \sin(V_j - g_j) = |H_j| \cos\ V_j - g_j - \frac{1}{4} \qquad \text{for} \qquad H_j \geq 0$$

$$= |H_j| \cos\ V_j - g_j - \frac{3}{4} \qquad \text{for} \qquad H_j < 0 \quad \ldots\ldots\ldots\ldots\ldots\ldots\ldots\ldots (2.10)$$

A similar adjustment of $\frac{1}{2}$ cycle is necessary for the annual, semi-annual, and semi-diurnal tidal constituents (only if the amplitude is negative).

Making these changes, the cluster contribution in the diurnal and terdiurnal cases is:

$$|H_j| \cos(V'_j - g_j) + \sum_k A_{jk} H_{jk} \cos(V'_{jk} + \alpha_{jk} - g_{jk}) + \sum_l A_{jl} H_{jl} \cos(V'_{jl} + \alpha_{jl} - g_{jl}) \quad \ldots\ldots\ldots (2.11)$$

where if $H_j < 0$, then $V' = V - \frac{3}{4}$, $\alpha_{jk} = \frac{1}{2}$, and $\alpha_{jl} = \frac{3}{4}$, and if $H_j > 0$, then $V' = V - \frac{1}{4}$, $\alpha_{jk} = 0$, and $\alpha_{jl} = \frac{1}{4}$. A further phase correction to the satellite tidal constituents is also required. Replacing H_{jk} and H_{jl} with their absolute values results in the following adjustment factors: $\alpha_{jk} = 0$ if both H_j and H_{jk} have the same sign, and $\alpha_{jk} = \frac{1}{2}$ otherwise; $\alpha_{jl} = \frac{1}{4}$ if both H_j and H_{jl} have the same sign, and $\alpha_{jl} = \frac{3}{4}$ otherwise. Similarly, for the annual, semi-annual, and semi-diurnal tidal constituents, the cluster contribution is written as:

$$|H_j| \cos(V'_j - g_j) + \sum_k A_{jk} |H_{jk}| \cos(V'_{jk} + \alpha_{jk} - g_{jk}) + \sum_l A_{jl} |H_{jl}| \cos(V'_{jl} + \alpha_{jl} - g_{jl}) \quad \ldots. (2.12)$$

where $V' = V + \frac{1}{2}$ if $H_j < 0$, and $V' = V$ otherwise; $\alpha_{jk} = 0$ if H_j and H_{jk} have the same sign, and $\alpha_{jk} = \frac{1}{2}$ otherwise; $\alpha_{jl} = -\frac{1}{4}$ if H_j and H_{jl} have the same sign, and $\alpha_{jl} = \frac{1}{4}$ otherwise.

When applying this cluster approach in a tidal analysis, it is assumed that the result found contains a nodal correction made to the main tidal constituents: $f_j H_j \cos(V'_j - g_j + u_j)$. For the purpose of calculating these nodal adjustment factors corresponding to the main tidal constituents, it is assumed that the admittance is nearly constant over the frequency range of the associated cluster. Thus, $g_j = g_{jk} = g_{jl}$, and $r_{jk} = |H_{jk}| / |H_j|$ and $r_{jl} = |H_{jl}| / |H_j|$ are equal to the ratios of the equilibrium amplitudes of the satellite tidal constituents to those of the major contributors. Dropping the prime notation (on V) and grouping the second- and third-order tidal potential terms into one summation (represented by the multiple jkl subscripts), the relationship between the analyzed results for a main tidal constituent and the actual cluster combination is represented by:

$$f_j |A_j| \cos(V_j - g_j + u_j) = |H_j| \cos(V_j - g_j) + \sum_k A_{jkl} r_{jkl} \cos(V_j + \alpha_{jkl} - g_j + \Delta_{jkl}) \quad \ldots . (2.13)$$

where $\Delta_{jkl} = V_{jkl} - V_j$. Expanding this result and observing that it holds for all $V_j(t)$, the following explicit formulas are found for the nodal factor and equilibrium argument, respectively (see Schureman [1941] and Schwiderski [1980]):

$$f_j = \left[1 + \sum_k A_{jk} r_{jk} \cos(\Delta_{jk} + \alpha_{jk}) \right]^2 + \left[\sum_k A_{jk} r_{jk} \sin(\Delta_{jk} + \alpha_{jk}) \right]^2 \Bigg]^{\frac{1}{2}} \quad \ldots . (2.14)$$

$$u_j = \arctan \frac{\sum_k A_{jk} r_{jk} \sin\left(\Delta_{jk} + \alpha_{jk}\right)}{1 + \sum_k A_{jk} r_{jk} \cos\left(\Delta_{jk} + \alpha_{jk}\right)} \qquad (2.15)$$

For a tidal analysis carried out over $2N + 1$ consecutive observations and sampled at Δt time intervals apart, the interaction-matrix element is given by (Foreman, 1977):

$$A_{jk} = \frac{\sin\left[(2N+1)\Delta t\left(\sigma_{jk} - \sigma_j\right)/2\right]}{(2N+1)\sin\left[\Delta t\left(\sigma_{jk} - \sigma_j\right)/2\right]} \qquad (2.16)$$

In the present study, historical water surface elevation data are obtained for the five water level gaging stations located within the interior of the Loxahatchee River estuary (see Figure 1.1). These water level data sets contain time-series water surface elevations (sampled at 30-minute intervals) corresponding to a two-year time period, which extends from January 1, 2003 to January 1, 2005, for these five water level gaging stations. (This two-year time period is chosen in order to include the project time period, which extends from October 1, 2003 to May 1, 2004.) Upon preliminary examination of these water surface elevation data, a significant amount of non-astronomical influence[§] appears to be included in the overall measured signals (see Appendix C). Thus, a harmonic analysis is performed on these water level data sets in order to extract the regular tidal oscillations from the total observed signals. A tidal analysis tool written in MATLAB computing language by Pawlowicz et al. (2002) is employed to accomplish this current task. This package of routines (collectively named T_TIDE) is used to perform a

---

[§] Non-astronomical influence refers to all non-astronomically driven physical processes which may affect coastal and oceanic water levels, including, but not limited to, temperature- and salinity-driven circulation, wind and pressure effects, and local resonant oscillations (i.e., seiches); however, within a semi-enclosed water body (e.g., an estuary), most non-astronomical influence may be attributed to meteorological effects.

classical tidal analysis on the historical water surface elevation data obtained at the five water level gaging stations located within the interior of the estuary.

While the classical tidal analysis approach employed by T_TIDE is fully described in Pawlowicz et al. (2002), the subsequent overview provides a brief summary of the procedure followed by the tidal analysis tool. The astronomical variables associated with the magnitude of the tidal potential (see Appendix A) are determined for a given Julian date using the formulas given by Seidelmann (1992). The effects produced by the tide-generating forces are then combined with the Doodson numbers (see Eq. [2.2]) to specify all possible tidal constituents. Following, the long-period, semi-diurnal, and diurnal tidal species are grouped into clusters (see Foreman [1977]), which are then collectively applied in the tidal analysis. Amplitude and phase estimates of the tidal constituents are made using a least-squares fitting procedure (see Eq. [2.5]) through algorithms described by Godin (1972) and Foreman (1977). A total of 146 tidal constituents may be chosen (according to the Rayleigh and Nyquist criteria) to include in the tidal analysis (see Foreman [1977]): 45 astronomical in origin; 101 shallow water-based. Lastly, phase corrections (see Eqs. [2.11] and [2.12]) and nodal adjustments (see Schureman [1941] and Schwiderski [1980]) are applied to the cluster contributions in order to determine the individual tidal constituents.

The historical tidal signal is then resynthesized over the project time period through the summation of Eq. (2.4) using the T_TIDE-computed tidal constituents and corresponding nodal adjustment factors (see Table 2.3). (Of importance, the solar annual [SA] and solar semi-annual [SSA] tidal constituents are excluded from this tidal resynthesis for the purpose of eliminating any seasonal variations within the resynthesized historical tidal signal.) Discrepancies between the historical water surface elevations and resynthesized historical tidal signals are apparent at all

five water level gaging stations (see Appendix C), indicating the presence of meteorology (see footnote on page 21) in the records of observations.

Table 2.3. 68 tidal constituents and corresponding nodal adjustment factors extracted by T_TIDE and used in the resynthesis of the historical tidal signal.

Tidal constituent[a]	Tidal species	Period (MSD)	Degrees per solar hour	Nodal factor (-)[b]	Equilibrium argument (rad)[b]
SA	long-period	365.18	0.0411	1.000	5.193
SSA	long-period	182.59	0.0822	1.000	1.415
MSM	long-period	31.81	0.4715	1.000	1.845
MM	long-period	27.55	0.5444	1.000	1.189
MSF	long-period	14.77	1.0159	1.000	3.034
MF	long-period	13.66	1.0980	1.000	4.450
ALP1	diurnal	1.211	12.3828	1.129	4.208
2Q1	diurnal	1.167	12.8543	1.122	6.048
SIG1	diurnal	1.160	12.9271	1.132	5.384
Q1	diurnal	1.120	13.3987	1.126	0.953
RHO1	diurnal	1.113	13.4715	1.159	0.264
O1	diurnal	1.076	13.9431	1.131	2.136
TAU1	diurnal	1.070	14.0252	0.837	0.437
BET1	diurnal	1.041	14.4145	1.156	0.874
NO1	diurnal	1.035	14.4967	1.104	1.619
CHI1	diurnal	1.030	14.5696	1.136	1.311
PI1	diurnal	1.006	14.9179	0.995	6.136
P1	diurnal	1.003	14.9589	0.994	5.043
S1	diurnal	1.000	15.0000	0.689	4.673
K1	diurnal	0.997	15.0411	1.080	3.216

Tidal constituent[a]	Tidal species	Period (MSD)	Degrees per solar hour	Nodal factor (-)[b]	Equilibrium argument (rad)[b]
PSI1	diurnal	0.995	15.0821	1.012	2.220
PHI1	diurnal	0.992	15.1232	0.941	4.764
THE1	diurnal	0.967	15.5126	1.136	4.988
J1	diurnal	0.962	15.5854	1.121	4.340
SO1	diurnal	0.934	16.0570	1.132	6.243
OO1	diurnal	0.929	16.1391	1.480	0.949
UPS1	diurnal	0.899	16.6835	1.508	2.214
OQ2	semi-diurnal	0.548	27.3510	0.875	1.669
EPS2	semi-diurnal	0.547	27.4238	0.937	1.054
2N2	semi-diurnal	0.538	27.8954	0.904	2.875
MU2	semi-diurnal	0.536	27.9682	0.966	2.269
N2	semi-diurnal	0.527	28.4397	0.974	4.126
NU2	semi-diurnal	0.526	28.5126	0.969	3.471
GAM2	semi-diurnal	0.519	28.9112	1.090	2.780
H1	semi-diurnal	0.518	28.9430	0.954	3.306
M2	semi-diurnal	0.518	28.9841	0.976	5.316
H2	semi-diurnal	0.517	29.0252	0.987	4.236
MKS2	semi-diurnal	0.516	29.0663	1.180	0.219
LDA2	semi-diurnal	0.509	29.4556	0.972	4.011
L2	semi-diurnal	0.508	29.5285	1.095	3.061
T2	semi-diurnal	0.501	29.9589	1.000	3.185
S2	semi-diurnal	0.500	30.0000	1.001	2.096
R2	semi-diurnal	0.499	30.0411	1.221	4.242
K2	semi-diurnal	0.499	30.0821	1.207	3.282
MSN2	semi-diurnal	0.491	30.5444	0.952	3.285
ETA2	semi-diurnal	0.490	30.6265	1.217	4.453
MO3	terdiurnal	0.349	42.9272	1.104	1.169

Tidal constituent[a]	Tidal species	Period (MSD)	Degrees per solar hour	Nodal factor (-)[b]	Equilibrium argument (rad)[b]
M3	terdiurnal	0.345	43.4762	0.965	4.828
SO3	terdiurnal	0.341	43.9430	1.132	4.232
MK3	terdiurnal	0.341	44.0252	1.054	2.249
SK3	terdiurnal	0.333	45.0411	1.082	5.312
MN4	fourth-diurnal	0.261	57.4238	0.950	3.159
M4	fourth-diurnal	0.259	57.9682	0.953	4.349
SN4	fourth-diurnal	0.257	58.4397	0.975	6.223
MS4	fourth-diurnal	0.254	58.9841	0.977	1.129
MK4	fourth-diurnal	0.254	59.0662	1.178	2.315
S4	fourth-diurnal	0.250	60.0000	1.003	4.193
SK4	fourth-diurnal	0.250	60.0821	1.209	5.379
2MK5	fifth-diurnal	0.205	73.0093	1.029	1.281
2SK5	fifth-diurnal	0.200	75.0411	1.083	1.125
2MN6	sixth-diurnal	0.174	86.4080	0.925	1.002
M6	sixth-diurnal	0.173	86.9523	0.930	3.382
2MS6	sixth-diurnal	0.171	87.9682	0.954	0.161
2MK6	sixth-diurnal	0.170	88.0503	1.150	1.348
2SM6	sixth-diurnal	0.169	88.9841	0.979	3.226
MSK6	sixth-diurnal	0.168	89.0662	1.180	4.411
3MK7	seventh-diurnal	0.147	101.9934	1.005	0.314
M8	eighth-diurnal	0.129	115.9364	0.908	2.414

[a] Refer to Appendix D for a listing of the tidal constituent amplitudes and phases.

[b] Nodal adjustment factors computed according to the 16th hour of November 1, 2003.

Meteorological effects (see footnote on page 21) contained within the records of observations are computed through Eq. (2.5) in order to quantify these discrepancies between the

historical water surface elevations and resynthesized historical tidal signals. Additionally, the solar annual (SA) and solar semi-annual (SSA) tidal constituents are resynthesized over the two-year time period associated with the historical water level data in order to obtain the seasonal variation contained within the overall measured signals. (This two-year time period is selected for the purpose of presenting two and four complete cycles of the annual and semi-annual seasonal variations, respectively.) Correlation between the computed meteorological residuals and resynthesized seasonal variations suggests that the observed water levels are highly influenced by long-term solar heating and weather effects (see footnote on page 21) (see Appendix E).

To close this discussion on tidal analysis, various harmonic equivalents (through use of the tidal constituents) of some non-harmonic terms are presented. A common non-harmonic term used to describe the tides is associated with the fortnightly modulation in the semi-diurnal tidal amplitudes, or the spring-neap tidal cycle (see Figure 2.1), which can be represented by the combination of the principal lunar (M2) and principal solar (S2) tidal constituents:

$$Z_0 + H_{M2}\cos\left(2\omega_1 t - g_{M2}\right) + H_{S2}\cos\left(2\omega_0 t - g_{S2}\right) \quad \ldots\ldots\ldots\ldots\ldots\ldots\ldots\ldots\ldots\ldots \quad (2.17)$$

where time zero is at syzygy (see Figure 2.1) and the angular speeds of the M2 and S2 tidal constituents, ω_1 and ω_0, respectively, can be found in Table 2.1. The maximum values of the combined amplitudes are given by mean high water springs and mean low water springs, respectively:

$$Z_0 + \left(H_{M2} + H_{S2}\right) \quad \ldots\ldots\ldots\ldots\ldots\ldots\ldots\ldots\ldots\ldots\ldots\ldots\ldots\ldots\ldots\ldots\ldots\ldots\ldots\ldots\ldots\ldots \quad (2.18)$$

$$Z_0 - \left(H_{M2} + H_{S2}\right) \quad (2.19)$$

and the minimum values of the combined amplitudes are given by mean high water neaps and mean low water neaps, respectively:

$$Z_0 + \left(H_{M2} - H_{S2}\right) \quad (2.20)$$

$$Z_0 - \left(H_{M2} - H_{S2}\right) \quad (2.21)$$

The relative importance of the diurnal and semi-diurnal tidal constituents may be expressed in terms of the form factor, as computed by the ratio of the major diurnal and semi-diurnal harmonic amplitudes:

$$FF = \frac{H_{K1} + H_{O1}}{H_{M2} + H_{S2}} \quad (2.22)$$

In terms of the form factor, the tides may be roughly classified as semi-diurnal (*FF* = 0.00 – 0.25), mixed/semi-diurnal (*FF* = 0.25 – 1.50), mixed/diurnal (*FF* = 1.50 – 3.00), or diurnal (*FF* > 3.00). Using the amplitudes of the K1, O1, M2, and S2 tidal constituents extracted in the harmonic analysis to compute the associated form factors, the tides in the Loxahatchee River estuary can be classified as slightly mixed and strongly semi-diurnal (see Table 2.4). To provide a relative basis, the form factors associated with the tides in the Western North Atlantic Tidal (WNAT) model domain are displayed in Figure 2.3.

Table 2.4. Computed form factors associated with the tides in the Loxahatchee River estuary.

Water level gaging station[a]	Tidal constituent amplitude (m)[b]				Form factor, *FF* (-)
	K1	O1	M2	S2	
Coast Guard Dock	0.060	0.050	0.323	0.047	0.298
Pompano Drive	0.064	0.051	0.321	0.045	0.314
Boy Scout Dock	0.058	0.048	0.308	0.046	0.300
Kitching Creek	0.058	0.048	0.313	0.048	0.293
River Mile 9.1	0.059	0.049	0.319	0.048	0.295

[a] Refer to Figure 1.1 for the locations of these five water level gaging stations.

[b] Refer to Appendix D for a listing of the tidal constituent amplitudes and phases.

Tides have also been classified in various other general ways that can be related to the tidal constituent amplitudes. One very crude classification of the tides that is still in use today is given as follows: tides with a range greater than 4 m are called macrotidal; those with a range between 2 and 4 m are called mesotidal; those with a range less than 2 m are called microtidal. Over the project time period, the range of the tides experienced at the five water level gaging stations located within the estuary varies between 0.50 and 1.00 m (see Appendix C). Thus, the tides within the Loxahatchee River estuary can be further classified as being microtidal.

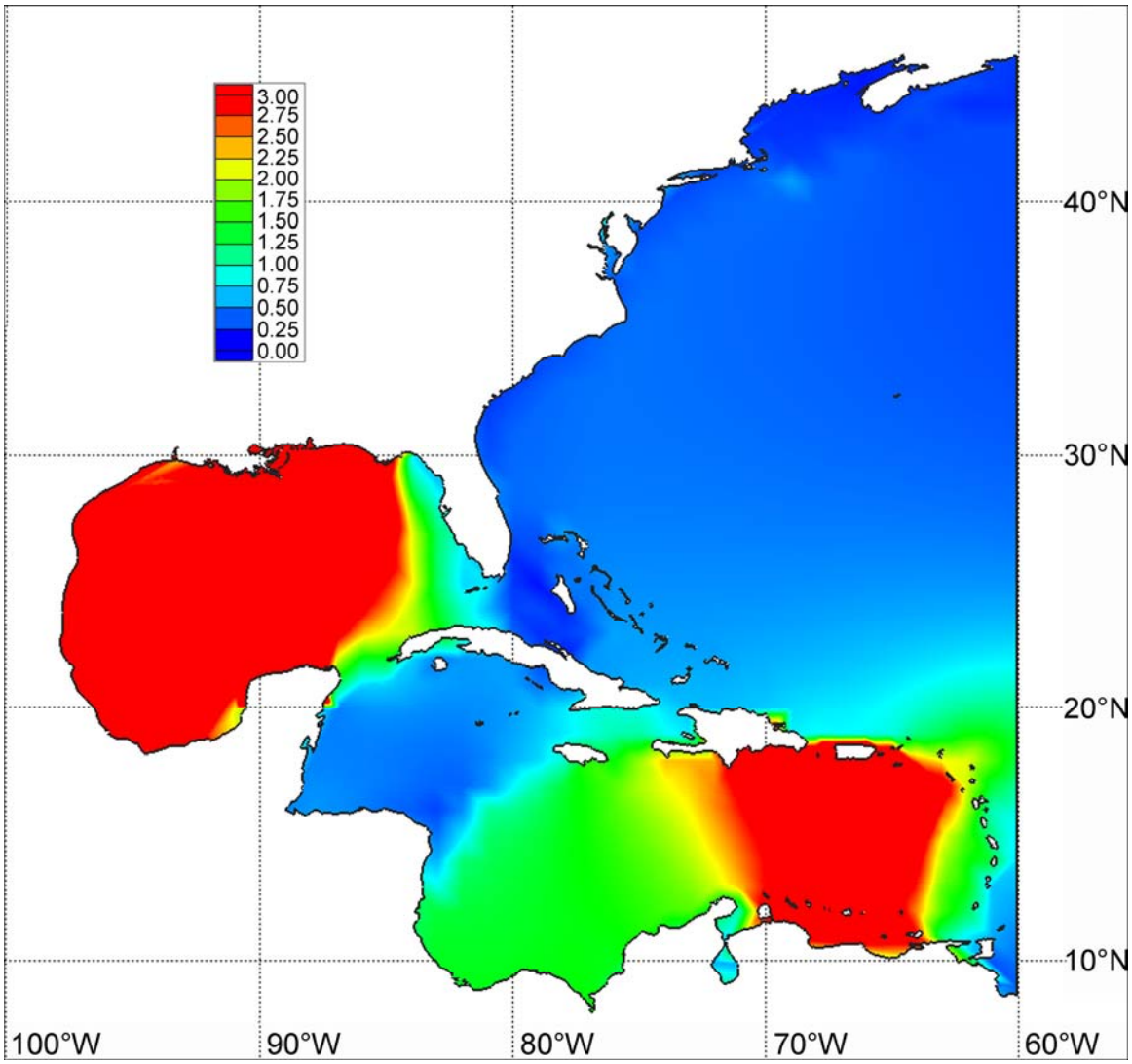

Figure 2.3. Computed form factors associated with the tides in the WNAT model domain, highlighting the diurnal ($FF \geq 3.00$) and semi-diurnal ($FF = 0.00 - 0.25$) tidal regimes experienced within the Gulf of Mexico and Caribbean Sea and in the western North Atlantic Ocean, respectively.